Crystal Structures and Electron Paramagnetic Resonance Spectra of $[Cu\{P(C_5H_4N)_3\}_2]Br_2\cdot 8H_2O$ and Cu^{2+}-Doped $[Zn\{P(C_5H_4N)_3\}_2]Br_2\cdot 8H_2O$, Examples of a Dynamic Jahn–Teller Effect in Two Dimensions†

Timothy Astley,[a] Henrietta Headlam,[a] Michael A. Hitchman,[a] F. Richard Keene,[b] John Pilbrow,[c] Horst Stratemeier,[a] Edward R. T. Tiekink[d] and Y. C. Zhong[c]

[a] *Chemistry Department, University of Tasmania, Box 252C, Hobart, Tasmania 7000, Australia*

[b] *Department of Molecular Sciences, James Cook University of North Queensland, Townsville, Queensland 4811, Australia*

[c] *Department of Physics, Monash University, Clayton, Victoria 3168, Australia*

[d] *Department of Chemistry, The University of Adelaide, Adelaide, South Australia 5005, Australia*

Crystals of $[Cu\{P(C_5H_4N)_3\}_2]Br_2\cdot 8H_2O$, studied at 173 K are triclinic, space group $P\bar{1}$, with unit-cell dimensions $a = 9.082(4)$, $b = 11.340(1)$, $c = 9.084(2)$ Å, $\alpha = 98.40(4)$, $\beta = 94.78(3)$, $\gamma = 98.27(7)°$ and $Z = 1$; those of $[Zn\{P(C_5H_4N)_3\}_2]Br_2\cdot 8H_2O$ studied at 293 K are monoclinic, space group $C2/m$ with $a = 12.506(6)$, $b = 13.588(7)$, $c = 11.593(7)$ Å, $\beta = 101.62(4)°$ and $Z = 2$. The structures were refined to final $R = 0.050$ for 3192 reflections with $I \geqslant 3.0\sigma(I)$, and $R = 0.033$ for 1737 reflections with $I \geqslant 3.0\sigma(I)$, respectively. The centrosymmetric copper complex has two Cu–N bonds [2.002(4) Å] considerably shorter than the other four [2.189(5) × 2, 2.191(5) Å × 2]. However, the temperature dependence of the EPR spectrum suggests that in fact the complex has a tetragonally elongated octahedral geometry with two possible orientations in the crystal lattice, these differing by interchange of the directions of the long and intermediate Cu–N bond directions. These forms are in dynamic equilibrium, with an activation energy of ≈600 cm^{-1} for the interchange. Analysis of the relative intensities of the EPR signals observed at ≈10 K suggests an energy difference between the structural isomers of ≈4 cm^{-1}. The zinc complex has crystallographic $2/m$ symmetry with two independent Zn–N distances [2.150(3) × 2; 2.187(3) Å × 4]. The temperature dependence of the EPR spectrum of this compound doped with ≈1% Cu^{2+} is similar to that of the pure copper(II) compound, but with a lower activation energy for interchange of the structural isomers. The dynamic behaviour of the copper(II) complex in the two compounds is discussed in terms of a potential surface obtained by considering the effects of Jahn–Teller coupling and lattice strain interactions. Bonding parameters derived from the electronic spectrum are consistent with the tetragonally elongated octahedral co-ordination geometry proposed.

Tripodal ligands involving nitrogen-donor heterocycles have been found to exhibit a number of useful properties in co-ordination and organometallic chemistry.[1] As part of a study of the electronic and steric characteristics of first-row transition-metal complexes of ligands of this kind[2–7] we have prepared the compounds $[M\{P(C_5H_4N)_3\}_2]Br_2\cdot 8H_2O$ (M = Cu or Zn) and report here their crystal structures. These indicate that one pair of *trans* M–N bonds is considerably shorter than the other two pairs. Such a ligand arrangement would be highly unusual for a copper(II) complex, as it implies the tetragonally compressed form of the Jahn–Teller distortion rather than the tetragonally elongated form almost invariably observed for six-co-ordinate complexes of this metal ion.[8] Although this has been previously reported for several compounds,[9] subsequent research has almost always found[10] that the compressed tetragonal geometry is in fact due to disorder of the long and one pair of short metal–ligand bonds of complexes which have the common tetragonally elongated octahedral co-ordination geometry. Electron paramagnetic resonance (EPR) spectroscopy[11] and extended X-ray absorption fine structure (EXAFS)[12] have both proved to be useful tools in resolving ambiguities of this kind, and we recently used these techniques to show[13] that the six crystallographically equivalent Cu–N bonds observed for the similar compound $[Cu\{CH(C_5H_4N)_3\}_2][NO_3]_2$ are in fact due to a three-dimensional disorder of the long and both pairs of short Cu–N bonds of a complex with a tetragonally elongated octahedral geometry.

The EPR spectrum of a complex exhibiting disorder can be particularly revealing, as the variation with temperature often provides information about the dynamics of the equilibrium between the structural isomers.[14] Recently, we developed a model to describe the potential surface of a six-co-ordinate copper(II) complex under the influence of Jahn–Teller coupling and perturbations due to the surrounding crystal lattice.[15] Initially, this was used to interpret the EPR spectra of the complexes formed when Cu^{2+} is doped into a range of diamagnetic host lattices,[16–18] though the model was later extended to treat the combined structural and EPR data available for pure copper(II) compounds,[19] and the situation where dynamic equilibria are influenced by pressure rather than temperature.[20]

The present paper reports the crystal structures and EPR spectra of $[Cu\{P(C_5H_4N)_3\}_2]Br_2\cdot 8H_2O$ and the analogous zinc(II) compound doped with ≈1% Cu^{2+}, and interprets these in terms of the potential surface and associated vibronic

† *Supplementary data available:* see Instructions for Authors, *J. Chem. Soc., Dalton Trans.*, 1995, Issue 1, pp. xxv–xxx.

Non-SI unit employed: G = 10^{-4} T.

wavefunctions of a copper(II) complex perturbed by Jahn–Teller coupling and 'strain' induced by the surrounding lattice.

Experimental

Syntheses.—The compound tris(2-pyridyl)phosphine was obtained using established methods.[4,21]

Bis[tris(2-pyridyl)phosphine]copper(II) nitrate, $[Cu\{P(C_5H_4N)_3\}_2][NO_3]_2$. A solution of $Cu(NO_3)_2\cdot 6H_2O$ (150 mg, 0.5 mmol) in acetone (5 cm^3) was added dropwise at room temperature to a stirred solution of tris(2-pyridyl)phosphine (265 mg, 1 mmol) in acetone (10 cm^3). The resulting suspension was cooled at 0 °C for 2 h, filtered, washed with acetone and air dried. Yield: 300 mg, 83%.

Bis[tris(2-pyridyl)phosphine]copper(II) bromide, $[Cu\{P(C_5H_4N)_3\}_2]Br_2\cdot 8H_2O$. The nitrate salt was converted into the bromide salt by anion-exchange chromatography using a QAE Sephadex A25 anion exchanger. Crystals grown by slow evaporation of an aqueous solution (Found: C, 40.4; H, 4.7; N, 9.4. Calc. for $C_{30}H_{40}Br_2CuN_6O_8P_2$: C, 40.1; H, 4.50; N, 9.4%).

Bis[tris(2-pyridyl)phosphine]zinc(II) nitrate, $[Zn\{P(C_5H_4N)_3\}_2][NO_3]_2$. A solution of $Zn(NO_3)_2\cdot 6H_2O$ (150 mg, 0.5 mmol) in acetone (5 cm^3) was added dropwise at room temperature to a stirred solution of tris(2-pyridyl)phosphine (250 mg, 1 mmol) in acetone (10 cm^3). The resulting suspension was cooled at 0 °C for 2 h, filtered, washed with acetone and air dried. Yield: 280 mg, 78%.

Bis[tris(2-pyridyl)phosphine]zinc(II) bromide, $[Zn\{P(C_5H_4N)_3\}_2]Br_2\cdot 8H_2O$. The nitrate salt was converted into the bromide salt by anion-exchange chromatography using a QAE Sephadex A25 anion exchanger. Crystals were grown by slow evaporation of an aqueous solution (Found: C, 40.2; H, 4.0; N, 9.6. Calc. for $C_{30}H_{40}Br_2N_6O_8P_2Zn$: C, 40.0; H, 4.5; N, 9.3%).

Spectroscopic Measurements.—The reflectance spectrum was recorded with a Beckmann DK2A spectrophotometer. The EPR spectra were measured at Q-band frequency, ≈34 GHz, over the temperature range 293–77 K using a JEOL JES-FE spectrometer equipped with a standard JEOL cryostat, crystal-rotation device and temperature controller. A crystal spectrum of the pure copper(II) compound was also measured at ≈10 K at X-band frequency (≈9.4 GHz) using a Varian E12 spectrometer. The crystal was cooled using an Oxford Instruments flow cryostat. An EPR spectrum of the powdered Cu^{2+}-doped zinc(II) compound was measured in the temperature range 4–100 K using a Bruker ESP 380E spectrometer operating at X-band. In each case the sample was prevented from losing water by covering it with a layer of EPR-inert silicone vacuum grease.

Crystallography.—Intensity data for a blue crystal of $[Cu\{P(C_5H_4N)_3\}_2]Br_2\cdot 8H_2O$ (173 K, 0.13 × 0.23 × 0.24 mm) and a pale yellow crystal of $[Zn\{P(C_5H_4N)_3\}_2]Br_2\cdot 8H_2O$ (293 K, diameter 0.5 mm) were measured on a Rigaku AFC6R diffractometer fitted with graphite-monochromatised Mo-Kα radiation, λ = 0.710 73 Å; the ω–2θ scan technique was employed to measure data such that θ_{max} was 27.5°. No decomposition of either crystal occurred during their respective data collections and only absorption-corrected data[22] which satisfied the criterion $I \geqslant 3.0\sigma(I)$ were used in the subsequent analyses. Crystal data are summarised in Table 1.

Each structure was solved by placing the metal atom on a crystallographic special site of symmetry and the remaining atoms were located from subsequent difference maps; the structures were refined by a full-matrix least-squares procedure based on F.[23] Non-hydrogen atoms were refined with anisotropic thermal parameters and H atoms were included in the models at their calculated positions (C–H 0.97 Å); water hydrogen atoms were not located. At convergence (σ weights, *i.e.* $1/\sigma^2(F)$ R = 0.050 and R' = 0.060 for the copper complex and R = 0.033 and R' = 0.037 for the zinc complex. The analysis of variace showed no special features in either case and the maximum peak in the final difference map was 0.71 and 0.43 e $Å^{-3}$ for the copper and zinc complexes, respectively. Scattering factors for all atoms were those incorporated in the TEXSAN program.[23] Fractional atomic coordinates are listed in Tables 2 and 5, anisotropic thermal parameters for the Cu^{2+} complex in Table 3, the numbering schemes shown in Figs. 1 and 2 which were drawn with the ORTEP program[24] with 50 and 30% probability ellipsoids, respectively and selected bond distances and angles are presented in Tables 4 and 6.

Additional material available from the Cambridge Crystallographic Data Centre comprises H-atom coordinates, thermal parameters and remaining bond lengths and angles.

Results and Discussion

Crystal Structures.—The structure of the cation in $[Cu\{P(C_5H_4N)_3\}_2]Br_2\cdot 8H_2O$ is shown in Fig. 1. The unit cell contains one formula unit of $[Cu\{P(C_5H_4N)_3\}_2]Br_2\cdot 8H_2O$, with the complex being disposed about a crystallographic centre of inversion. As expected for a structure of this type there are significant intermolecular contacts in the lattice; however, these contacts do not involve the cation but the bromide anion and the water molecules of crystallisation. The bromide atom forms three hydrogen-bonding contacts to the solvent water molecules [Br···O(2), O(4), O(3) are 3.291(4), 3.324(5), 3.326(5) Å, respectively] and, as well, there are water–water contacts involving each of the four water molecules. In the CuN_6 octahedral cation there are two classes of Cu–N contacts with the Cu–N(21) and Cu–N(31) distances of 2.189(5) and 2.191(5) Å being equal within experimental error and significantly longer than the Cu–N(11) distance of 2.002(4) Å; other parameters within the complex cation are as expected. The co-ordination geometry about the copper(II) atom, with two short and four long Cu–N distances, is thereby unusual, the compound appearing to conform to the rare *compressed* form of the tetragonal Jahn–Teller distortion.[8] Such a geometry would be remarkable, since previous reports[9] of such a stereochemistry have almost invariably been found to be fallacious;[10] as far as we are aware $KAlCuF_6$ remains the only example of a compound involving just one ligand type where all available evidence[25,26] suggests a compressed tetragonal Jahn–Teller distortion. As shown in the following section, the EPR evidence

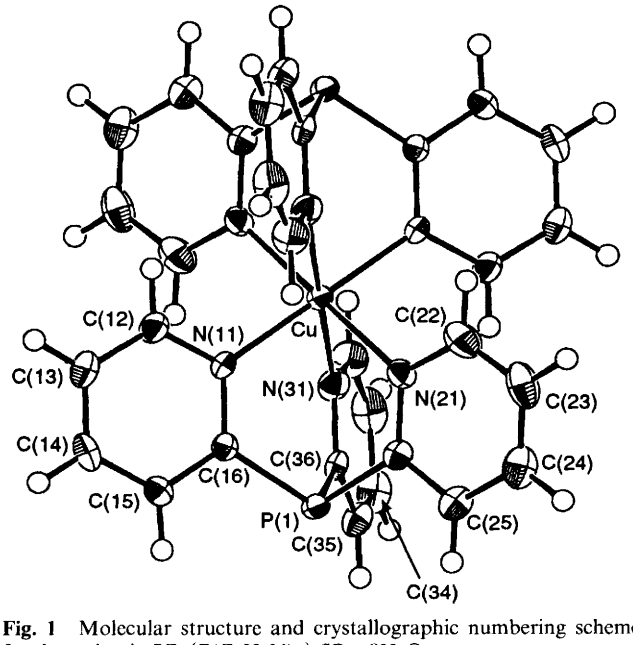

Fig. 1 Molecular structure and crystallographic numbering scheme for the cation in $[Cu\{P(C_5H_4N)_3\}_2]Br_2\cdot 8H_2O$

Table 1 Crystal data for $[M\{P(C_5H_4N)_3\}_2]Br_2\cdot 8H_2O$ (M = Cu **1** or Zn **2**)

Compound	**1**	**2**
Formula	$C_{30}H_{40}Br_2CuN_6O_8P_2$	$C_{30}H_{40}Br_2N_6O_8P_2Zn$
M	898.0	899.8
Crystal system	Triclinic	Monoclinic
Space group	$P\bar{1}$	$C2/m$
a/Å	9.082(4)	12.506(6)
b/Å	11.40(1)	13.588(7)
c/Å	9.084(2)	11.593(7)
α/°	98.40(4)	
β/°	94.78(3)	101.62(4)
γ/°	98.27(7)	
U/Å^3	915.4(9)	1929(1)
Z	1	2
D_c/g cm^{-3}	1.629	1.549
μ/cm^{-1}	28.49	28.49
Maximum, minimum transmission factors	1.033, 0.948	1.153, 0.842
$F(000)$	455	912
No. data measured	4669	2417
No. unique data	4398	2313
No. observed data [$I \geqslant 3.0\sigma(I)$]	3192	1737
R	0.050	0.033
R'	0.060	0.037

Table 2 Fractional atomic coordinates for the non-hydrogen atoms of $[Cu\{P(C_5H_4N)_3\}_2]Br_2\cdot 8H_2O$

Atom	x	y	z
Br	0.616 80(6)	0.328 13(5)	0.616 77(6)
Cu*	0	0	0
P(1)	0.276 0(2)	−0.011 6(1)	0.275 9(2)
O(1)	0.846 9(4)	0.499 6(4)	0.152 2(4)
O(2)	0.888 9(4)	0.359 9(3)	0.889 3(4)
O(3)	−0.581 8(5)	0.416 8(5)	−0.108 1(6)
O(4)	0.891 5(5)	0.416 6(5)	0.418 4(5)
N(11)	0.128 8(4)	0.141 5(4)	0.128 3(5)
N(21)	0.203 6(5)	−0.079 4(4)	−0.027 3(5)
N(31)	−0.027 8(5)	−0.079 7(4)	0.203 3(5)
C(12)	0.108 3(6)	0.251 1(5)	0.108 0(6)
C(13)	0.191 4(7)	0.352 8(5)	0.191 5(7)
C(14)	0.298 6(6)	0.342 0(5)	0.298 7(6)
C(15)	0.320 8(6)	0.229 8(5)	0.320 7(6)
C(16)	0.234 3(5)	0.131 9(4)	0.235 2(5)
C(22)	0.225 9(7)	−0.135 5(6)	−0.160 3(7)
C(23)	0.341 1(7)	−0.200 2(6)	−0.180 2(7)
C(24)	0.433 2(7)	−0.208 8(6)	−0.060 1(7)
C(25)	0.413 0(6)	−0.149 7(5)	0.078 3(6)
C(26)	0.297 5(6)	−0.086 3(5)	0.089 6(6)
C(32)	−0.159 7(6)	−0.135 9(6)	0.225 8(7)
C(33)	−0.179 7(7)	−0.200 0(6)	0.340 1(8)
C(34)	−0.059 6(7)	−0.208 1(6)	0.433 8(7)
C(35)	0.077 6(6)	−0.150 1(5)	0.412 9(6)
C(36)	0.089 8(6)	−0.085 7(4)	0.298 5(6)

* Atom has site occupancy factor = 0.5.

strongly suggests that in $[Cu\{P(C_5H_4N)_3\}_2]Br_2\cdot 8H_2O$ the longer Cu–N bonds actually represent the *average* ligand positions of one pair of closely bonded pyridines (Cu–N ≈2.04 Å), and one pair of loosely bound amines (Cu–N ≈2.34 Å), so that the local co-ordination geometry about the copper(II) in fact conforms to that generally observed for this metal ion.

The Cu–N distances proposed for $[Cu\{P(C_5H_4N)_3\}_2]Br_2\cdot 8H_2O$ are quite similar to those observed for complexes of other similar tripod ligands, for instance 1.994, 2.020 and 2.385 Å in the compound $[Cu\{CH(C_5H_4N)(pz)_2\}_2][NO_3]_2$, where pz = pyrazol-1-yl.[6] However, the overall Jahn–Teller distortion is somewhat larger than that suggested by the bond lengths 2.04 (×4) and 2.25 (×2) Å revealed by EXAFS of the compound $[Cu\{CH(C_5H_4N)_3\}_2][NO_3]_2$.[13]

Although $[Zn\{P(C_5H_4N)_3\}_2]Br_2\cdot 8H_2O$ has a similar stoichiometry and co-ordination geometry to the above copper(II) compound, it crystallises in the monoclinic space group $C2/m$. The molecular structure of the cation is shown in Fig. 2. In the lattice, there are three contacts between the bromide anion and symmetry-related water molecules of solvation [*i.e.* Br ··· O(3), O(1), O(1′) 3.333(4), 3.356(4), 3.356(4) Å, respectively] and water–water interactions involving all water molecules. The geometry about the zinc atom, which is located at a crystallographic site of symmetry $2/m$, is distorted octahedral, the Zn–N(11) distances being 2.150(3) Å (×2) and Zn–N(21) 2.187(3) Å (×4). However, the difference in bond lengths is much smaller than for the copper(II) complex (≈0.03 compared with ≈0.19 Å) because of the absence of the Jahn–Teller effect. Also, because of the higher site symmetry, the two longer Zn–N bonds are crystallographically equivalent, and this has implications for the EPR spectrum of Cu^{2+} doped into the zinc compound (see following section).

EPR Spectra.—At 293 K the EPR spectrum of powdered $[Cu\{P(C_5H_4N)_3\}_2]Br_2\cdot 8H_2O$ is characteristic of a tetragonal g tensor with $g_{\parallel} = 2.04$, $g_{\perp} = 2.165$. On cooling to 77 K, although the *average* g value remains unchanged, the $g_{\perp}$ signal is largely replaced by resonances corresponding to $g = 2.09$ and 2.25, so that at low temperature the overall spectrum is that expected for a complex with a tetragonally elongated octahedral geometry with a slight orthorhombic distortion. Except that the change occurs at higher temperature, this behaviour is reminiscent of that observed for the centre $[Cu(H_2O)_2Cl_4]^{2-}$ in Cu^{2+}-doped NH_4Cl.[18] Here, a 'reversed' g tensor of tetragonal symmetry is replaced by a 'normal' g tensor of orthorhombic symmetry at a temperature of ≈30 K, and this was explained by the complex having a tetragonally elongated octahedral geometry, but with the long bonds fluctuating between the Cu–Cl directions. Above ≈30 K the rate of exchange between the 'structural isomers' is more rapid than the EPR time-scale, but when the temperature drops below ≈30 K the $[Cu(H_2O)_2Cl_4]^{2-}$ complex becomes 'frozen' into one orientation.

The behaviour of $[Cu\{P(C_5H_4N)_3\}_2]Br_2\cdot 8H_2O$ can therefore be explained if the complex has an essentially tetragonally elongated octahedral geometry, though with the long bonds randomly distributed between two of the three Cu–N bond directions. The different orientations are almost energetically equivalent, so that upon input of energy the direction of tetragonal elongation may 'switch' from one bond to another. At low temperature this switching is relatively slow, and the EPR spectrum is that expected for an orthorhombically

Table 3 Anisotropic thermal parameters for $[Cu\{P(C_5H_4N)_3\}_2]Br_2\cdot 8H_2O$*

Atom	U_{11}	U_{22}	U_{33}	U_{12}	U_{13}	U_{23}
Br	0.0279(3)	0.0291(3)	0.0284(3)	0.0035(2)	0.0006(2)	0.0026(2)
Cu	0.0180(4)	0.0189(5)	0.0183(5)	0.0042(4)	0.0011(4)	0.0033(4)
P(1)	0.0207(7)	0.0219(7)	0.0209(7)	0.0057(5)	0.0005(5)	0.0048(6)
O(1)	0.034(2)	0.037(2)	0.032(2)	0.005(2)	0.011(2)	0.002(2)
O(2)	0.031(2)	0.026(2)	0.034(2)	0.008(2)	−0.000(2)	0.007(2)
O(3)	0.039(3)	0.069(4)	0.057(3)	0.017(2)	0.010(2)	−0.005(3)
O(4)	0.053(3)	0.069(4)	0.044(3)	−0.005(3)	0.010(2)	0.018(3)
N(11)	0.019(2)	0.017(2)	0.022(2)	0.006(2)	0.004(2)	0.004(2)
N(21)	0.034(3)	0.023(2)	0.018(2)	0.005(2)	0.001(2)	0.001(2)
N(31)	0.021(2)	0.026(3)	0.036(3)	0.005(2)	0.002(2)	0.004(2)
C(12)	0.029(3)	0.021(3)	0.031(3)	0.005(2)	0.001(2)	0.007(2)
C(13)	0.038(3)	0.020(3)	0.039(3)	0.007(3)	0.006(3)	0.007(3)
C(14)	0.031(3)	0.022(3)	0.027(3)	−0.004(2)	0.008(2)	−0.005(2)
C(15)	0.021(3)	0.026(3)	0.020(3)	0.002(2)	0.005(2)	0.001(2)
C(16)	0.018(2)	0.020(3)	0.018(3)	0.005(2)	0.006(2)	0.002(2)
C(22)	0.046(4)	0.042(4)	0.024(3)	0.003(3)	0.003(3)	−0.000(3)
C(23)	0.049(4)	0.034(4)	0.032(3)	0.000(3)	0.018(3)	−0.005(3)
C(24)	0.041(4)	0.034(4)	0.038(4)	0.010(3)	0.021(3)	0.007(3)
C(25)	0.030(3)	0.029(3)	0.029(3)	0.007(2)	0.010(2)	0.010(2)
C(26)	0.024(3)	0.021(3)	0.023(3)	0.003(2)	0.006(2)	0.008(2)
C(32)	0.022(3)	0.034(3)	0.050(4)	−0.000(3)	0.003(3)	0.003(3)
C(33)	0.030(3)	0.034(4)	0.052(4)	−0.003(3)	0.017(3)	−0.002(3)
C(34)	0.041(4)	0.030(3)	0.041(4)	0.006(3)	0.020(3)	0.008(3)
C(35)	0.031(3)	0.027(3)	0.032(3)	0.011(2)	0.010(2)	0.008(3)
C(36)	0.023(3)	0.016(3)	0.025(3)	0.008(2)	0.006(2)	0.002(2)

* Anisotropic thermal parameter given by the expression $T_{aniso} = \exp[-2\pi^2(h^2a^{*2}U_{11} + k^2b^{*2}U_{22} + l^2c^{*2}U_{33} + 2hka^*b^*U_{12} + 2hla^*c^*U_{13} + 2klb^*c^*U_{23})]$.

Table 4 Selected bond distances (Å) and angles (°) for $[Cu\{P(C_5H_4N)_3\}_2]Br_2\cdot 8H_2O$

Cu–N(11)	2.002(4)	Cu–N(21)	2.189(5)
Cu–N(31)	2.191(5)	P(1)–C(16)	1.813(5)
P(1)–C(26)	1.819(5)	P(1)–C(36)	1.820(5)
N(11)–C(12)	1.326(6)	N(11)–C(16)	1.334(6)
N(21)–C(22)	1.328(7)	N(21)–C(26)	1.324(6)
N(31)–C(32)	1.321(7)	N(31)–C(36)	1.334(6)
N(11)–Cu–N(21)	87.5(2)	N(11)–Cu–N(31)	87.8(2)
N(11)–Cu–N(21')*	92.5(2)	N(11)–Cu–N(31')	92.2(2)
N(21)–Cu–N(31)	89.7(2)	N(21)–Cu–N(31')	90.3(2)
C(16)–P(1)–C(26)	100.9(2)	C(16)–P(1)–C(36)	100.6(2)
C(26)–P(1)–C(36)	99.9(2)	Cu–N(11)–C(12)	118.9(3)
Cu–N(11)–C(16)	123.5(3)	C(12)–N(11)–C(16)	117.6(4)
Cu–N(21)–C(22)	120.1(4)	Cu–N(21)–C(26)	121.4(4)
C(22)–N(21)–C(26)	118.0(5)	Cu–N(31)–C(32)	120.6(4)
Cu–N(31)–C(36)	121.2(4)	C(32)–N(31)–C(36)	117.8(5)

* Primed atoms are related by a centre of inversion.

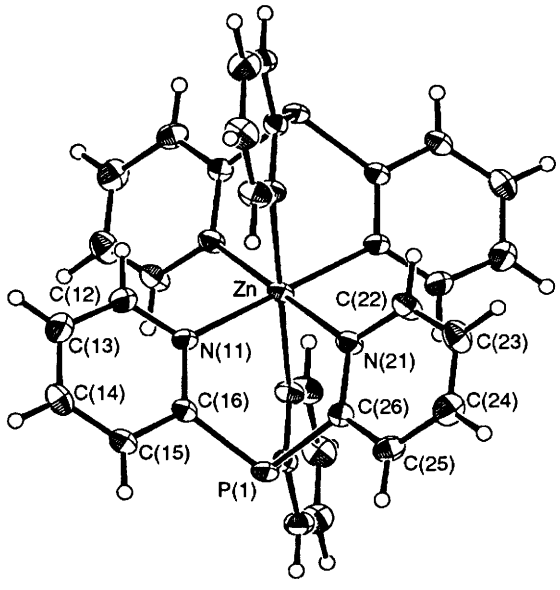

Fig. 2 Molecular structure and crystallographic numbering for the cation in $[Zn\{P(C_5H_4N)_3\}_2]Br_2\cdot 8H_2O$

distorted tetragonally elongated complex with the direction of the long axis of each complex fixed in space. However, at room temperature, the rate of switching is faster than the EPR time-scale, so that the signals associated with the long and one pair of short bonds are averaged to give the $g_\perp$ signal.

This picture was confirmed by measuring the EPR spectrum of a single crystal at 77 K. In general, two symmetry-related signals were observed, despite the fact that the triclinic cell contains only one $[Cu\{P(C_5H_4N)_3\}_2]^{2+}$ complex. The positions of the signals varied with the crystal orientation, and they coalesced at the orientation producing the minimum g value (2.04). It may be assumed that here the magnetic field is parallel to the short Cu–N(11) bond. The variation of the g values in the plane normal to this direction is shown in Fig. 3. Two similar sinusoidal curves occur, with extrema 90° apart. A hyperfine splitting of 160×10^{-4} cm^{-1} due to coupling with the copper nuclear spin was observed for the signals associated with the higher g values. The maximum and minimum g values, $g_3 = 2.25$, $g_2 = 2.09$, are identical to the molecular g values observed in the powder spectrum at 77 K. The two sets of signals thus correspond to two possible orientations of a complex having an orthorhombically distorted tetragonally elongated geometry, one having the long bond to N(21), and the other with this to N(31). For one of the curves in Fig. 3 the maximum and minimum g values occur when the magnetic field lies close to the Cu–N(21) and Cu–N(31) bond directions, respectively, while the reverse is true for the other curve.

Upon raising the temperature the signals corresponding to the two possible orientations coalesce at ≈140 K (Fig. 4). At this temperature, the energy difference between the signals, measured in frequency units, approximately equals the rate of

Table 5 Fractional atomic coordinates for the non-hydrogen atoms of $[Zn\{P(C_5H_4N)_3\}_2]Br_2\cdot 8H_2O$

Atom	x	y	z
Br(1)[a]	0.619 84(4)	0	0.328 11(5)
Zn[b]	0	0	0
P(1)[a]	0.275 52(8)	0	−0.015 1(1)
O(1)	0.155 6(2)	0.265 7(2)	0.419 1(3)
O(2)[a]	0	0.151 9(3)	0.5
O(3)[a]	0.890 8(3)	0	0.360 3(3)
N(11)[a]	0.136 1(3)	0	0.146 6(3)
N(21)	0.086 1(2)	0.112 3(2)	−0.081 2(2)
C(12)[a]	0.119 7(4)	0	0.257 7(4)
C(13)[a]	0.203 6(4)	0	0.354 9(4)
C(14)[a]	0.309 6(4)	0	0.339 4(4)
C(15)[a]	0.327 7(3)	0	0.225 1(4)
C(16)[a]	0.240 7(3)	0	0.131 7(4)
C(22)	0.032 1(2)	0.188 9(2)	−0.137 3(3)
C(23)	0.078 0(3)	0.257 5(2)	−0.199 7(3)
C(24)	0.185 2(3)	0.246 8(2)	−0.206 2(3)
C(25)	0.243 5(3)	0.168 9(2)	−0.148 2(3)
C(26)	0.192 9(2)	0.103 3(2)	−0.086 5(2)

[a] Atom has site occupancy factor = 0.5. [b] Atom has site occupancy factor = 0.25.

Table 6 Selected bond distances (Å) and angles (°) for $[Zn\{P(C_5H_4N)_3\}_2]Br_2\cdot 8H_2O$

Zn–N(11)	2.150(3)	Zn–N(21)	2.187(3)
P(1)–C(16)	1.841(4)	P(1)–C(26)	1.837(3)
N(11)–C(12)	1.344(5)	N(11)–C(16)	1.352(5)
N(21)–C(22)	1.337(4)	N(21)–C(26)	1.356(3)
N(11)–Zn–N(21)	87.73(9)	N(11)–Zn–N(21′)	92.27(9)
N(21)–Zn–N(21″)	88.5(1)	N(21)–Zn–N(21‴)	91.5(1)
C(16)–P(1)–C(26)	101.6(1)	C(26)–P(1)–C(26″)	99.6(2)
Zn–N(11)–C(12)	120.5(3)	Zn–N(11)–C(16)	122.1(3)
C(12)–N(11)–C(16)	117.4(4)	Zn–N(21)–C(22)	120.6(2)
Zn–N(21)–C(26)	122.1(2)	C(22)–N(21)–C(26)	117.0(3)

Primed atoms related by the symmetry operation $-x, -y, -z$, doubly primed ones by $x, -y, z$ and triply primed ones by $-x, y, -z$.

exchange R_{exch} between the two orientations, equation (1).[27,†]

$$R_{exch} \approx |g_2 - g_3|\beta B\pi/(\sqrt{2}h) \quad (1)$$

Here, β is the Bohr magneton and h Planck's constant, and substituting $g_2 = 2.09$, $g_3 = 2.25$ and the average magnetic field of the signals $B = 1.15$ T into equation (1) yields the rate $R \approx 5.7 \times 10^9$ s^{-1}. Since the energy difference between the structural isomers, ΔE, is clearly small compared with the energy barrier ΔE^*, the latter may be estimated from the rate expression (2)[28] where k is the Boltzmann constant, R the gas constant and T the absolute temperature. Substitution of the above exchange rate, together with the temperature of coalescence $T \approx 140$ K, into equation (2) yields the estimate $\Delta E^* \approx 607$ cm^{-1}.

$$R_{exch} \approx kT[\exp(-\Delta E^*/RT)]/h \quad (2)$$

The fact that the activation energy is so high means that at low temperature the complexes will be 'frozen' into the less-stable orientation. When the sample is cooled rapidly, as in the present case, this non-equilibrium situation will occur at approximately the temperature at which the cooling rate becomes comparable to the rate of exchange between the orientations. Assuming a cooling rate of 1K s^{-1}, and

† Note that the frequency ω in ref. 27 is given in rad s^{-1}. This may be converted into the frequency in Hz, ν, *via* the relationship $\omega = 2\pi\nu$.

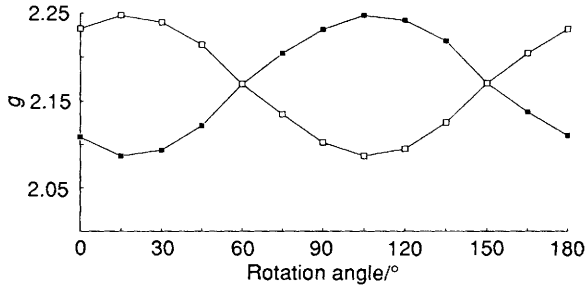

Fig. 3 Plot of g_1 (■) and g_2 (□) as a function of the rotation of the direction of the magnetic field in the plane normal to the Cu–N(11) direction in a crystal of $[Cu\{P(C_5H_4N)_3\}_2]Br_2\cdot 8H_2O$ at 77 K

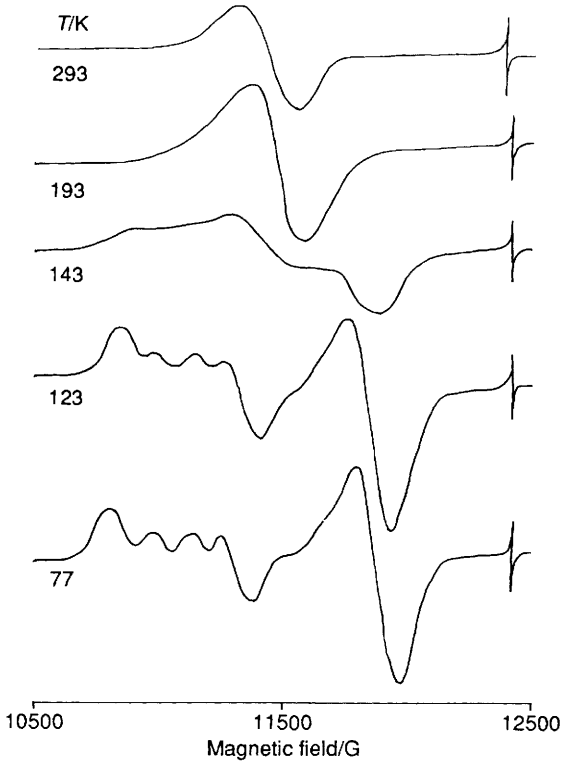

Fig. 4 Q-Band EPR spectra at various temperatures of a crystal of $[Cu\{P(C_5H_4N)_3\}_2]Br_2\cdot 8H_2O$ with the magnetic field parallel to the Cu–N(21) or Cu–N(31) direction. The weak, sharp resonance at ≈0.13 T is due to finely ground diphenylpicrylhydrazyl (dpph)

substituting this for R_{exch} in equation (2), suggests the complex will be 'frozen' into a particular distribution of orientations at $T \approx 27$K, the estimate being quite insensitive to the rate of cooling. In agreement with this, the single-crystal EPR spectra measured at X-band frequency at ≈10 K still showed two signals for most orientations of the magnetic field, though these were no longer equal in intensity. The relative intensity of each signal is expected to be proportional to the fractional number of complexes having that orientation, so that the ratio of the intensities is equal to the ratio P of the populations of the two states. When the complexes are in equilibrium, P depends upon the energy difference ΔE between the two states *via* expression (3).[29] The spectra when the magnetic field is approximately

$$P = \exp(\Delta E/RT) \quad (3)$$

parallel to the Cu–N(21) and Cu–N(31) directions are shown in Fig. 5, from which it may be seen that the signal corresponding to $g = 2.25$ is relatively more intense than that at $g = 2.09$ for one direction of the magnetic field, while the reverse is true for

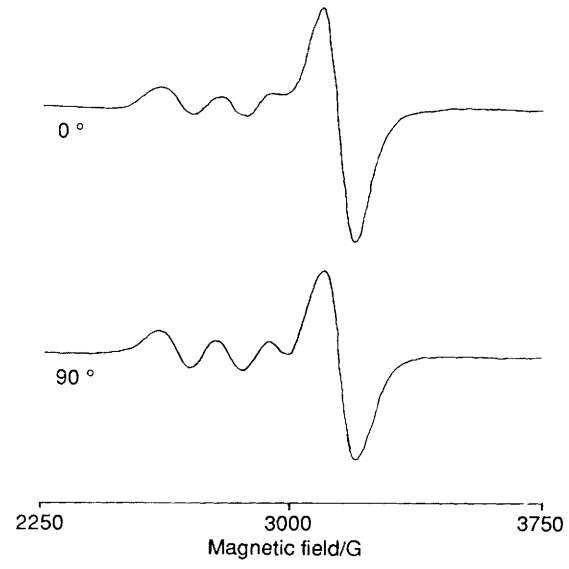

Fig. 5 X-Band EPR spectra of a crystal of $[Cu\{P(C_5H_4N)_3\}_2]Br_2 \cdot 8H_2O$ with the magnetic field parallel to the Cu–N(21) and Cu–N(31) directions (which orientation corresponds to which direction is unknown)

the other. Unfortunately, because of the poorly defined morphology of the crystals, it was not possible to determine which signal is associated with each bond direction. The ratio of the intensities was estimated to be $\approx 0.83:1$ and substitution of this in equation (3) together with the temperature $T \approx 27$ K at which the complexes are 'frozen' into the two states yields the value $\Delta E \approx 3.5$ K for the energy difference between the orientational isomers. A similar slight intensity difference between the signals was still apparent in the spectra measured at 77 K. The ratio of signal intensities was $\approx 0.93:1$ and substitution into equation (3) yields $\Delta E \approx 3.9$ K. Considering the rather large uncertainties involved, the self-consistency of the two estimates is pleasing.

The temperature dependence observed for the EPR spectrum of a powdered sample of $[Zn\{P(C_5H_4N)_3\}_2]Br_2 \cdot 8H_2O$ doped with $\approx 1\%$ Cu^{2+} is quite similar to that of the pure compound, except that a change from the pattern associated with a 'reversed' to a 'normal' g tensor occurred at ≈ 50 K. The spectra observed at Q band at 293 and 77 K, and at X band over the range 120–20 K, are shown in Fig. 6. The Q-band spectra yield the values $g_{\|} = 2.042$, $g_{\perp} = 2.165$ for the high-temperature exchange-narrowed g tensor. For the low-temperature spectrum, only the highest g value may be resolved at $g = 2.255$; the resonances due to the other two g values presumably contribute to the broad inflection at ≈ 0.34 T (Fig. 6). Assuming that the $g_{\perp}$ signal in the exchange-narrowed spectrum splits symmetrically in the low-temperature spectrum, while the lowest g value is temperature independent, leads to the estimates $g_1 = 2.04$, $g_2 = 2.08$, $g_3 = 2.26$ for the molecular g values of Cu^{2+}-doped $[Zn\{P(C_5H_4N)_3\}_2]Br_2 \cdot 8H_2O$, these being virtually identical to those of the pure copper(II) complex. Hyperfine splittings of 85×10^{-4} and 160×10^{-4} cm^{-1} were observed above and below the transition temperature, the latter being identical to that seen for the pure complex, and very similar to the values observed for analogous complexes with tetragonally elongated octahedral geometries.[6,7] At low temperature additional structure was observed, presumably due to coupling with the nitrogen nuclei, but this was too poorly resolved to be worthy of analysis (Fig. 6). Substitution of the appropriate parameters $g_2 = 2.08$, $g_3 = 2.26$, $T = 50$, $B = 0.33$T into equations (1) and (2) yields the value $\Delta E^* \approx 220$ cm^{-1} for the activation energy of the interchange of the long and intermediate bond directions for the copper(II) guest complex.

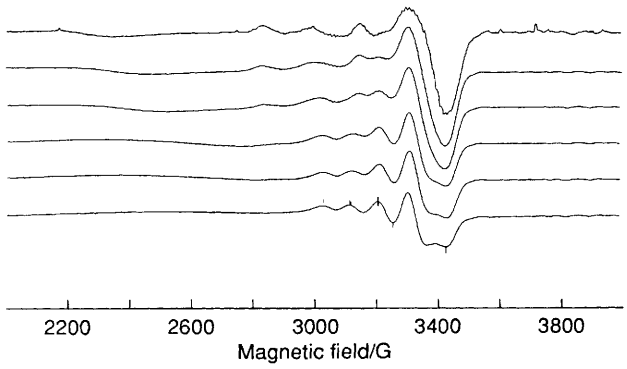

Fig. 6 X-Band EPR spectra of a powder of $[Zn\{P(C_5H_4N)_3\}_2]Br_2 \cdot 8H_2O$ doped with $\approx 1\%$ Cu^{2+} measured at temperatures of (from top to bottom) 20, 40, 50, 60, 80 and 120 K

This is considerably lower than the corresponding value for the pure copper(II) compound, and the possible reasons are discussed in the following section.

Potential Surface of the Complex.—The energy levels of a six-co-ordinate copper(II) complex are conventionally described in terms of the coupling between the ^2E_g electronic state and the e_g Jahn–Teller active vibration.[15] To first order, a complex with six identical ligands undergoes a radial distortion ρ in the e_g mode to yield the 'Mexican hat' potential surface shown in Fig. 7(*a*). Here, E_{JT} represents the Jahn–Teller stabilisation energy. At this level of approximation, the Q_θ and Q_ε components of the vibration, pictured in Fig. 7(*b*), are equivalent, and the energy minimum is a circular well of radius ρ with the geometry and concomitant electronic wavefunction specified by the angle φ. Higher-order effects distort this surface, producing three minima which almost invariably occur at $\varphi = 0$, 120 and 240°, corresponding to octahedral geometries tetragonally elongated along z, x and y, respectively, and the unpaired electron in a $d_{x^2-y^2}$ type orbital. Saddlepoints corresponding to compressed tetragonal geometries, and d_{z^2} type electronic wavefunctions, occur at $\varphi = 60$, 180 and 300°, the energy difference between the minima and saddlepoints being defined as 2β. When the ligands are inequivalent, either inherently or due to interactions with the surrounding crystal lattice, this is normally expressed by a 'strain' characterised by axial and equatorial components S_θ and S_ε, respectively. The strain shifts both the positions and relative energies of the minima, and it is the dynamic equilibrium between the vibronic levels of such surfaces that gives rise to temperature-dependent effects of the kind discussed here.[15] A model based on these concepts has been able to account quantitatively for the temperature dependence of the EPR spectra and geometries of a range of dynamic copper(II) complexes,[16–20] and it is of interest to apply this to the present complex.

The procedure used to calculate the potential surface has been described in detail previously.[16–18] The basic potential surface of the $[Cu\{P(C_5H_4N)_3\}_2]^{2+}$ complex is best defined by considering the g values at low temperature. Although in principle the metal hyperfine parameters may be treated in a similar fashion, here the interpretation is complicated by the fact that these depend not only on the orbital angular momentum of the unpaired electron, but also on the 'contact' interaction between the s-electron density and the nuclear spin. Since the primary interest is in the dynamics of the system the hyperfine coupling has therefore not been considered in the present treatment.

The overall Jahn–Teller distortion is largely decided by the balance between the force constant f of the e_g mode and the linear coupling constant A_1. For the present complex the former was assumed to be similar to that reported[17] for the $[Cu(H_2O)_6]^{2+}$ ion, where $h\nu = 300$ cm^{-1}. Assuming that the distortion

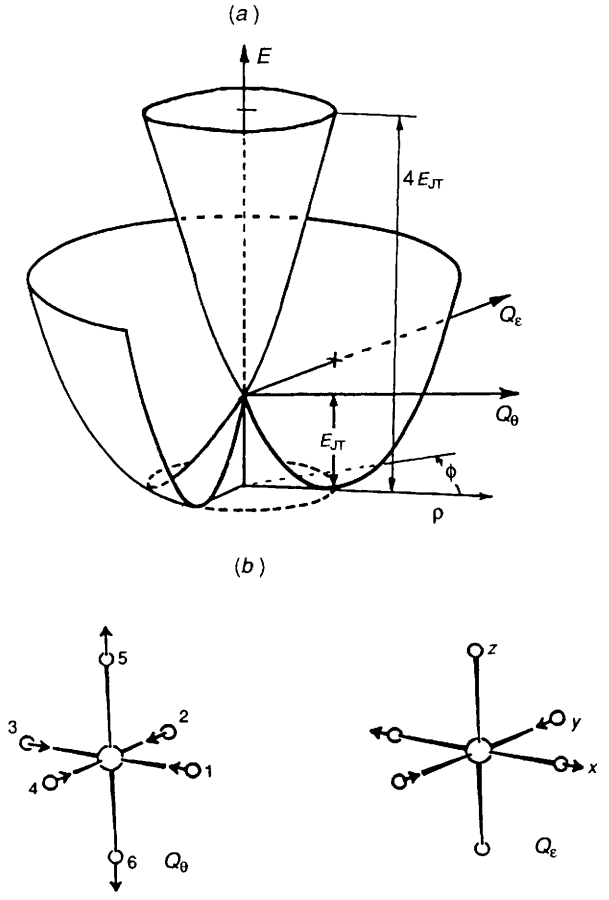

Fig. 7 (*a*) 'Mexican hat' potential surface formed by $e_g \times E_g$ Jahn–Teller coupling. (*b*) Form of the two components of the e_g Jahn–Teller active vibration

involves motion of the pyridine group as a whole, so that the effective mass M is 78, the energy of the e_g mode may be estimated as $h\nu = 140\ cm^{-1}$ from the relationship (4). The value

$$h\nu = \sqrt{(f/M)}/0.001\ 722 \qquad (4)$$

of A_1 may be obtained from the relationship (5) (see ref. 16 for a

$$A_1 = (2h\nu E_{JT})^{\frac{1}{2}} \qquad (5)$$

discussion of the units used to define the various parameters). The Jahn–Teller stabilisation energy E_{JT} [Fig. 7(*a*)] can be estimated approximately from the energy ΔE of the transition between the split levels of the ^2E_g state of the parent octahedral complex,[14] equation (6). The reflectance spectrum of

$$\Delta E \approx 4E_{JT} + 2|S_\theta| \qquad (6)$$

$[Cu\{P(C_5H_4N)_3\}_2]Br_2 \cdot 8H_2O$ is shown in Fig. 8. This consists of a band at 15 500 cm^{-1} with a shoulder at $\approx$17 000 cm^{-1} which may be assigned to transitions to the split components of the $^2T_{2g}$ level of the parent octahedral complex, and a shoulder at $\approx$8500 cm^{-1} which is due to the transition between the levels derived from the $d_{x^2-y^2}$ and d_{z^2} orbitals. The sharper peaks at lower energy are assigned as infrared overtones; similar peaks are observed in the reflectance spectrum of the corresponding zinc(II) compound (Fig. 8). Substitution of $\Delta E = 8500\ cm^{-1}$ into equation (6), and anticipating the value $S_\theta \approx -660\ cm^{-1}$, gives $E_{JT} = 1795\ cm^{-1}$, and substitution of this into equation (5) yields the estimate $A_1 = 700\ cm^{-1}$.

The position of the minimum in the 'trough' of the warped Mexican-hat potential surface depends upon the balance

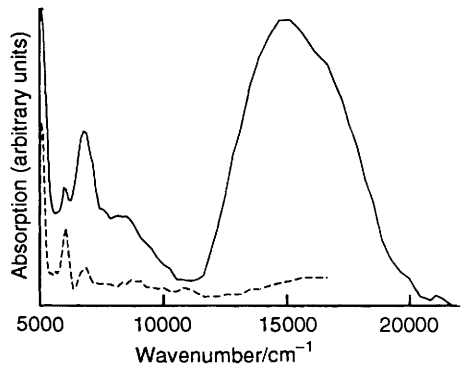

Fig. 8 Reflectance spectrum of powdered $[Cu\{P(C_5H_4N)_3\}_2]Br_2 \cdot 8H_2O$ at 293K (full line); the spectrum of $[Zn\{P(C_5H_4N)_3\}_2]Br_2 \cdot 8H_2O$ (dashed line) is shown in the lower-energy region to indicate the positions of the infrared overtones

between the lattice strain, which in the present case favours a compressed tetragonal geometry, and the warping parameter β, which is a measure of the tendency of the strain-free complex to prefer a tetragonally elongated geometry. It has been shown[30] that the former geometry will only become stable when $|S_\theta| > \approx 9\beta$. An axially symmetric strain of lower magnitude, relative to β, will produce a pair of equivalent minima each corresponding to an orthorhombic geometry.[30] The calculation of the low-temperature orthorhombic g tensor of $[Cu\{P(C_5H_4N)_3\}_2]Br_2 \cdot 8H_2O$ thus provides a means of estimating the ratio of S_θ to β reasonably accurately. The absolute values of the parameters may be obtained only approximately. For the pure complex the large activation energy for the exchange between the two lowest vibronic wavefunctions, $\approx$600 cm^{-1}, indicates a high degree of warping of the potential surface, with $\beta > \approx 300\ cm^{-1}$ (the barrier height for a warped potential surface in the absence of lattice strain effects is $\approx 2\beta$). The axial strain S_θ acts along the Cu–N(11) direction, and raises in energy the third minimum in the potential surface, that which corresponds to the long bonds of the tetragonally elongated complex lying along this direction. As thermal population of the well would cause an increase in the g value along this bond direction, its temperature invariance over the range 4–293 K provides a lower limit of $\approx -400\ cm^{-1}$ for the parameter S_θ (the negative sign corresponds to a compression). The parameter S_ε represents the amount by which lattice interactions render the other two minima in the surface inequivalent in energy. These correspond to the long Cu–N bonds occurring to N(21) and N(31), and *vice versa*, and as this energy difference is very small, $\approx 4\ cm^{-1}$, S_ε must also be quite modest, $\approx 2\ cm^{-1}$.

Reasonable agreement with the experimental data is obtained with vibronic wavefunctions calculated using the values $\beta = 507\ cm^{-1}$, $S_\theta = -660$ and $S_\varepsilon = 3\ cm^{-1}$. The g values of the lowest vibronic level, $g_1 = 2.054\ (2.04)$, $g_2 = 2.080\ (2.09)$, $g_3 = 2.251\ (2.25)$, agree well with the experimental values (in parentheses) of the more intense set of signals observed at low temperature. The effects of covalency were included by means of orbital-reduction parameters $k_1 = 0.84$, $k_2 = 0.83$, $k_3 = 0.74$. The electronic components of the vibronic wavefunctions are linear combinations of the $d_{x^2-y^2}$ and d_{z^2} orbitals $ad_{x^2-y^2} - bd_{z^2}$, and the resulting wavefunctions are of the form[31] (7). The

$$\Psi = cx^2 + ey^2 + fz^2 \qquad (7)$$

expectation values of the squares of the parameters c, e and f normalised to unity give the relative probability that the unpaired electron will be found along the x, y or z cartesian axis. For the lowest wavefunction the parameters are $\langle c^2 \rangle = 0.0026$, $\langle e^2 \rangle = 0.4664$ and $\langle f^2 \rangle = 0.5310$ so that the unpaired electron essentially occupies a $d_{z^2-y^2}$ orbital, with a slight admixture of d_{x^2}. The unconventional labelling of the orbitals

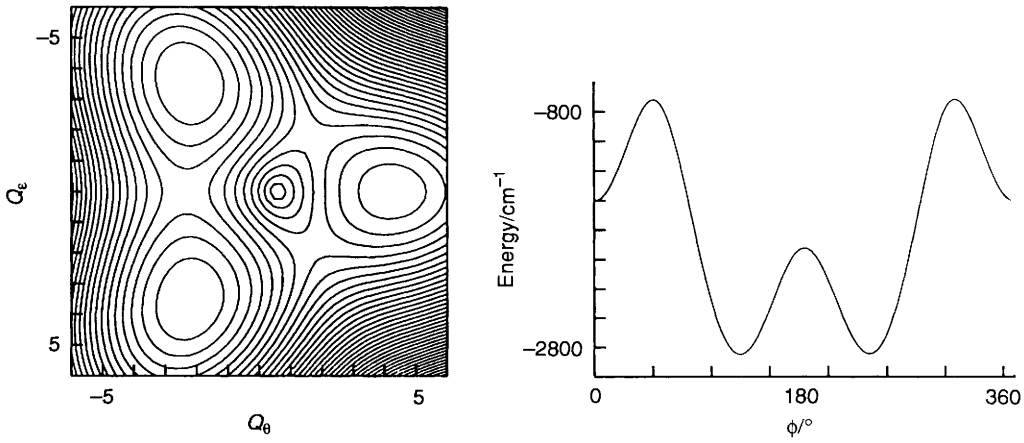

Fig. 9 Left: contour energy plot of the lower region of the potential surface calculated for $[Cu\{P(C_5H_4N)_3\}_2]Br_2\cdot 8H_2O$ (the spacing between each curve represents 100 cm^{-1} and Q_θ and Q_ε have dimensionless units; see ref. 18). Right: variation of the potential energy as a function of co-ordination geometry at a fixed Jahn–Teller radius (see text for details). The parameters defining the potential surface are: $A_1 = 700\ cm^{-1}$, $\beta = 505\ cm^{-1}$, $S_\theta = -660\ cm^{-1}$, $S_\varepsilon = 3\ cm^{-1}$, $h\nu = 140\ cm^{-1}$, $M = 78$

occurs because z defines the symmetry axis of the axial strain. Since this corresponds to a compression it is expected to coincide with the direction of the shortest Cu–N bond, Cu–N(11). The bond lengths calculated as described previously[19,20] (1.98, 2.04, 2.37 Å) represent only approximate estimates, since these depend upon the ligand mass. This was taken as that of a single pyridine group, 78, and coupling with internal vibrations of the tripod ligand was ignored. Nevertheless, the calculated value of Cu–N(11) agrees reasonably well with that observed experimentally, 2.002 Å, while the average calculated for the two longer bonds, 2.20 Å, is similar to the distances observed for Cu–N(21) and Cu–N(31), 2.189 and 2.191 Å.

The second lowest level lies at 4.8 cm^{-1}, with g values which are essentially identical to those of the lowest level, but with g_2 and g_3 reversed. These correspond to the values derived from the less-intense set of signals observed at low temperature (values in parentheses). The electronic wavefunction parameters $\langle c^2\rangle = 0.4662$, $\langle e^2\rangle = 0.0026$ and $\langle f^2\rangle = 0.5312$ conform to this pattern, with the magnitudes of $\langle c^2\rangle$ and $\langle e^2\rangle$ being interchanged, as do the calculated bond lengths.

A contour-energy plot of the lower region of the potential surface, and the variation of the energy minimum as a function of the angle φ at a constant Jahn–Teller radius $\rho = A_1/h\nu$, are shown in Fig. 9. The high value of β means that the surface is strongly warped, with the lower-energy vibronic wavefunctions highly localised in the minima. The barrier height between the lower pair of minima is very high, which is consistent with the activation energy for exchange between the two lowest wavefunctions, $\Delta E^* \approx 600\ cm^{-1}$. In agreement with this, the first vibronic wavefunction to be significantly delocalised over the two lower minima occurred at $\approx 700\ cm^{-1}$.

The g values of the $[Cu\{P(C_5H_4N)_3\}_2]^{2+}$ complex formed when Cu^{2+} is doped into $[Zn\{P(C_5H_4N)_3\}_2]Br_2\cdot 8H_2O$ are essentially identical to those of the pure compound, implying that the lowest pair of vibronic wavefunctions are very similar in the two lattices. However, exchange between these involves a much lower activation energy, $\Delta E^* \approx 220\ cm^{-1}$, for the 'doped' complex, suggesting that here delocalisation of the vibronic wavefunctions occurs at significantly lower energy. One factor contributing to this is the higher symmetry of the zinc(II) lattice. Since the Zn–N(21) and Zn–N(31) bonds are crystallographically equivalent the orthorhombic component of the lattice strain is formally zero. In the absence of random strains due to lattice imperfections, this means that even the lowest pair of vibronic wavefunctions are delocalised over the two minima. In practice, as first recognised by Ham,[32] small random strains make the wells at each lattice site inequivalent, and act to localise the vibronic wavefunctions. Little experimental evidence is available on the size of the random strains present in different lattices, and estimates have ranged from ≈ 1.5 to 10^{-5} cm^{-1}.[18,32] To investigate this point, it was assumed that the random strains could be represented by a single average value, and calculations were performed for S_ε ranging from 2 to 10^{-5} cm^{-1} with all other parameters identical to those used for pure $[Cu\{P(C_5H_4N)_3\}_2]Br_2\cdot 8H_2O$. For the lowest pair of levels, for all values of S_ε the vibronic wavefunctions were strongly localised, one in each of the two lower wells of the potential surface, and g values similar to those observed experimentally were obtained in each case. However, for very small of values the random strain, delocalisation over the two lowest minima in the potential surface occurred for quite low-lying upper vibronic levels. For $S_\varepsilon = 10^{-5}$ cm^{-1}, the first significantly delocalised level occurred at 237 cm^{-1}, quite similar to the activation energy $\Delta E^* \approx 220\ cm^{-1}$ estimated for the rate of exchange between the lowest pair of levels in the Cu^{2+}-doped complex.

Plots of the square of the vibrational part of the vibronic wavefunctions are shown for the first, second, seventh and eighth vibronic wavefunctions, calculated on the one hand using the value of the orthorhombic strain, $S_\varepsilon = 3\ cm^{-1}$, estimated for pure $[Cu\{P(C_5H_4N)_3\}_2]Br_2\cdot 8H_2O$ [Fig. 10(*a*)], and on the other using an estimate of $S_\varepsilon = 10^{-5}\ cm^{-1}$ to represent the random strains present in Cu^{2+}-doped $[Zn\{P(C_5H_4N)_3\}_2]Br_2\cdot 8H_2O$ [Fig. 10(*b*)]. For the pure copper compound, the wavefunctions are highly localised, with the maxima alternating in the two wells as the energy increases. For the doped complex, while the lower pair of levels are strongly localised, the seventh and eighth wells are significantly delocalised. Thus, the lower energy barrier to the interchange between the 'structural isomers' in the doped complex, compared with the pure compound, is most likely due to the greater delocalisation of the upper vibronic wavefunctions which occurs when the orthorhombic component of the lattice strain is very small.

It is to be expected that a broadly similar lattice strain to that which acts on the guest copper(II) complex will also be present in the zinc(II) compound. Assuming a similar energy for the e_g vibration, and correcting for the difference in average metal–ligand bond distance, the estimate $S_\theta = -660\ cm^{-1}$ derived from the above analysis of the EPR spectrum implies the bond lengths Zn–N 2.145 (×2), 2.190 (×4) Å for the corresponding zinc compound, in excellent agreement with the values observed crystallographically, Zn–N(11) 2.150(3) (×2), Zn–N(12) 2.187(3) (×4) Å. The same value of S_θ was derived for the pure and doped copper(II) complexes, and this confirms that despite

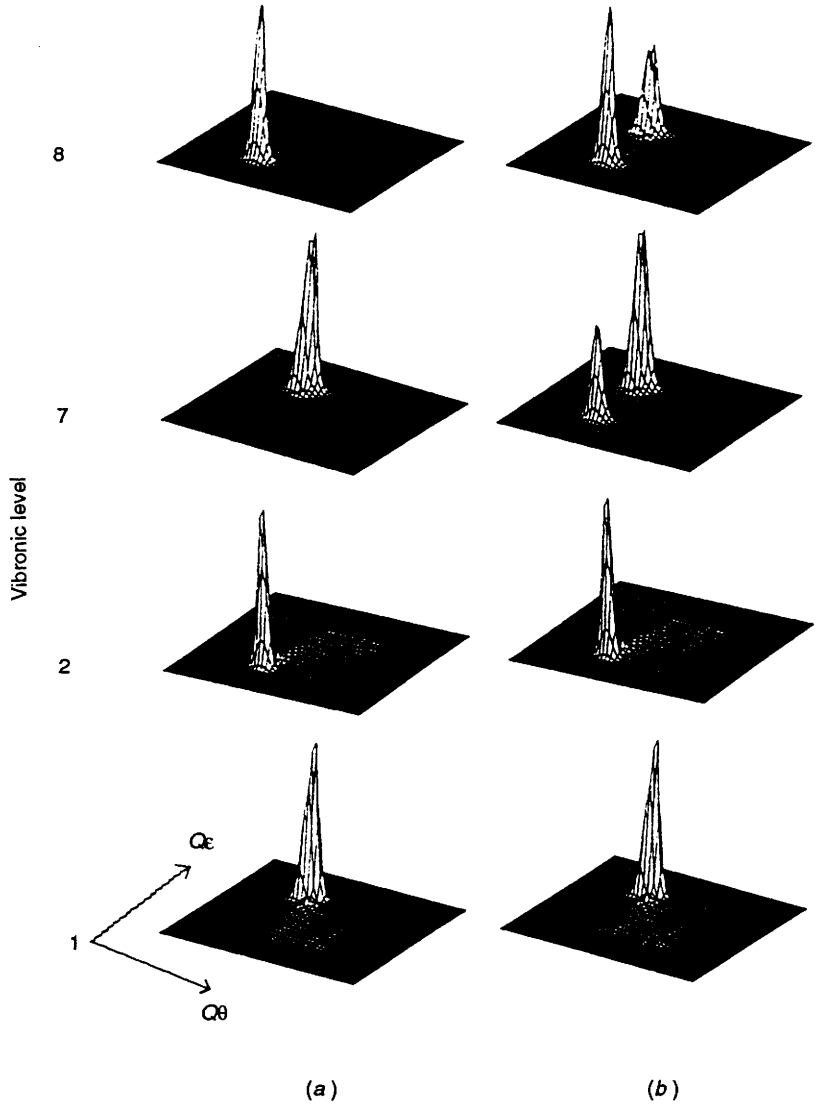

Fig. 10 Plots of the square of the vibrational part of the vibronic wavefunctions for the first, second, seventh and eighth levels of (*a*) $[Cu\{P(C_5H_4N)_3\}_2]Br_2 \cdot 8H_2O$ and (*b*) the copper complex in Cu^{2+}-doped $[Zn\{P(C_5H_4N)_3\}_2]Br_2 \cdot 8H_2O$

the difference in the crystal structure the lattice interactions in the copper(II) and zinc(II) compounds are very similar.

Bonding Parameters.—The above model implies that at the local level each complex in $[Cu\{P(C_5H_4N)_3\}_2]Br_2 \cdot 8H_2O$ has a tetragonally elongated octahedral geometry, with a slight orthorhombic distortion, rather than the compressed tetragonal geometry indicated by the X-ray diffraction results, and it is of interest to consider the implications of this on the metal–ligand interactions. These are conveniently described using the angular overlap model of the bonding in metal complexes.[33] The transition energies expected for the complex were investigated using the computer program CAMMAG developed by Gerloch and co-workers.[34] This calculates the transition energies by assigning angular overlap model σ- and π-bonding parameters e_σ, $e_{\pi x}$, $e_{\pi y}$ to each ligand, and summing the metal–ligand interactions using an angular-overlap matrix defined by the crystal structure of the complex. In the present case, the structure was assumed to be similar to that of the complex in $[Cu\{CH(C_5H_4N)(pz)_2\}_2][NO_3]_2$, where the Cu–N bond distances[6] are quite close to those derived for $[Cu\{P(C_5H_4N)_3\}_2]Br_2 \cdot 8H_2O$ in the above calculations. Bonding parameters based upon those reported[13] for the pyridine groups in the complex $[Cu\{CH(C_5H_4N)_3\}_2][NO_3]_2$, $e_\sigma = 5800\,cm^{-1}$, $e_{\pi y} = 900\,cm^{-1}$, were used in the calculation. These values relate to a Cu–N bond length of 2.04 Å, and to take into account the somewhat different geometry of the present complex it was assumed the bonding parameters are inversely proportional to the fifth power of the metal–ligand bond distance, as in other studies.[35] For the disordered Cu–N bonds, the distances derived in the calculations (2.038 and 2.365 Å) were used to make these corrections. The $e_{\pi x}$ parameter, which defines the π bonding in the plane of the pyridine ring, was assumed negligible, as in studies with other similar ligands.[6,7] An additional parameter e_{ds} to describe the configuration interaction with the metal 4s orbital,[36] was used. This was set to one quarter the value of e_σ, the approximate ratio observed for a range of planar complexes.[37] The following calculated transition energies are reasonably close to those observed experimentally (given in parentheses): 7500 (7800); 15 050 (15 500); 17 300, 18 200 (18 000) cm^{-1}. The g values $g_1 = 2.040$, $g_2 = 2.066$, $g_3 = 2.233$, calculated using an isotropic orbital reduction parameter $k = 0.80$ and effective spin–orbit coupling constant $\lambda = 590\,cm^{-1}$, are also in reasonable agreement with the experimental values ($g_1 = 2.04$, $g_2 = 2.09$, $g_3 = 2.25$). Moreover, the bonding parameters derived for the ligand are quite similar to those estimated for pyridine groups in analogous tripod ligands.[6,7,13] It should be noted that transition energies calculated in an analogous manner, but using the bond lengths of the compressed tetragonal geometry

implied by the crystal structure of the complex (4600; 13 600; 15 600, 16 500 cm^{-1}), are in poor agreement with those observed experimentally. The angular overlap model calculations thus confirm the conclusions of the above model, that at the local level the copper(II) complex in $[Cu\{P(C_5H_4N)_3\}_2]Br_2 \cdot 8H_2O$ has a tetragonally elongated octahedral geometry, rather than the tetragonally compressed geometry implied by the crystal-structure analysis.

Conclusion

Although the crystal structure of $[Cu\{P(C_5H_4N)_3\}_2]Br_2 \cdot 8H_2O$ measured at 173 K indicates Cu–N bond distances which imply a tetragonally compressed octahedral co-ordination geometry, the EPR spectrum suggests that at the local level each complex has a tetragonally elongated octahedral geometry with a slight orthorhombic distortion. The shortest Cu–N bonds always occur to one pair of nitrogen atoms, but the intermediate and long Cu–N bonds are randomly distributed between the other two pairs of nitrogen atoms. The two arrangements of the copper(II) complex differ in energy by only ≈ 4 cm^{-1}, so that at temperatures above ≈ 100 K the number of complexes adopting each orientation is almost equal, and it is the *average* of the two bond lengths which is observed in the crystal-structure analysis. The energy barrier to 'switching' of the two pairs of bonds is quite high, ≈ 600 cm^{-1}, so that on cooling to below ≈ 27 K complexes in the higher-energy orientation become 'frozen' into this orientation. The crystal structure of $[Zn\{P(C_5H_4N)_3\}_2]Br_2 \cdot 8H_2O$ is similar to that of the corresponding copper(II) compound in that two Zn–N bonds are shorter than the other four, but in this case the four longer bonds are crystallographically equivalent. At low temperature the g values of the copper(II) complex formed by doping $\approx 1\%$ Cu^{2+} into the zinc(II) compound are identical to those of the pure compound, suggesting a similar geometry for the 'guest' copper complex. However, the energy barrier to interchange of the two possible orientations of this guest complex is considerably smaller than that for the pure compound. This is probably because the very small energy difference between the orientations at any particular site, produced by random strains in the lattice, causes significant delocalisation of low-lying vibronic wavefunctions.

Acknowledgements

We are grateful to Mr. Richard Bowen and Dr. Sue Berners-Price (Griffith University, Brisbane) for a gift of a sample of tris(2-pyridyl)phosphine. Dr. Malcolm Gerloch of the University of Cambridge is thanked for making available the computer program CAMMAG. The assistance of Dr. Barry O'Grady of the University of Tasmania in estimating the rate of exchange between the structural isomers is gratefully acknowledged. Financial support (to M. A. H., J. P., F. R. K. and E. R. T. T.) was provided by the Australian Research Council.

References

1 S. Trofimenco, *Chem. Rev.*, 1972, **72**, 497; *Prog. Inorg. Chem.*, 1986, **34**, 115.
2 T. A. Hafeli and F. R. Keene, *Aust. J. Chem.*, 1988, **41**, 1379.
3 P. S Moritz, A. A. Diamantis, F. R. Keene, M. R. Snow and E. R. T. Tiekink, *Aust. J. Chem.*, 1988, **41**, 1352.
4 F. R. Keene, M. R. Snow, P. J. Stephenson and E. R. T. Tiekink, *Inorg. Chem.*, 1988, **27**, 2040.
5 P. A. Anderson, F. R. Keene, E. Horn and E. R. T. Tiekink, *Appl. Organomet. Chem.*, 1990, **4**, 523.
6 T. Astley, A. J. Canty, M. A. Hitchman, G. L. Rowbottom, B. W. Skelton and A. H. White, *J. Chem. Soc., Dalton Trans.*, 1991, 1981.
7 T. Astley, J. M. Gulbis, M. A. Hitchman and E. R. T. Tiekink, *J. Chem. Soc., Dalton Trans.*, 1993, 509.
8 See B. J. Hathaway, *Struct. Bonding (Berlin)*, 1984, **57**, 55.
9 K. Knox, *J. Chem. Phys.*, 1959, **30**, 991.
10 C. Friebel and D. Reinen, *Z. Anorg. Allg. Chem.*, 1974, **407**, 193.
11 H. Stratemeier, B. Wagner, E. R. Krausz, R. Lindner, H.-H. Schmidtke, J. Pebler, W. E. Hatfield, L. ter Haar, D. Reinen and M. A. Hitchman, *Inorg. Chem.*, 1994, **33**, 2320.
12 P. J. Ellis, H. C. Freeman, M. A. Hitchman, D. Reinen and B. Wagner, *Inorg. Chem.*, 1994, **33**, 1249.
13 T. Astley, P. J. Ellis, H. C. Freeman, M. A. Hitchman, F. R. Keene and E. R. T. Tiekink, *J. Chem. Soc., Dalton Trans.*, 1995, 595.
14 D. Reinen and M. Atanasov, *Magn. Reson. Rev.*, 1991, **15**, 167.
15 M. A. Hitchman, *Comments Inorg. Chem.*, 1994, **15**, 197.
16 M. J. Riley, M. A. Hitchman and D. Reinen, *Chem. Phys.*, 1986, **102**, 11.
17 M. J. Riley, M. A. Hitchman and A. wan Mohammed, *J. Chem. Phys.*, 1987, **87**, 3766.
18 M. J. Riley, M. A. Hitchman, D. Reinen and G. Steffen, *Inorg. Chem.*, 1988, **27**, 1924.
19 J. Bebendorf, H. B. Bürgi, E. Gamp, M. A. Hitchman, D. Reinen, M. J. Riley and H. Stratemeier, unpublished work.
20 C. J. Simmons, M. A. Hitchman, H. Stratemeier and A. J. Schultz, *J. Am. Chem. Soc.*, 1993, **115**, 11304.
21 R. J. Bowen, S. Berners-Price and I. D. Jenkins, unpublished work.
22 N. Walker and D. Stuart, *Acta Crystallogr., Sect. A*, 1983, **39**, 158.
23 TEXSAN, Structure Analysis Package, Molecular Structure Corporation, Houston, TX, 1992.
24 C. K. Johnson, ORTEP II, ORNL Report 5136, Oak Ridge National Laboratory, Oak Ridge, TN, 1976.
25 G. Wingefeld and R. Hoppe, *Z. Anorg. Allg. Chem.*, 1984, **516**, 223.
26 M. Atanasov, M. A. Hitchman, R. Hoppe, K. S. Murray, B. Mourbaraki, D. Reinen and H. Stratemeier, *Inorg. Chem.*, 1993, **32**, 3397.
27 A. Carrington and A. D. McLachlan, *Introduction to Magnetic Resonance*, Harper and Row, New York, 1967, p. 207.
28 K. J. Laidler, *Chemical Kinetics*, 3rd edn., Harper and Row, New York, 1987, p. 94.
29 B. Silver and D. Getz, *J. Chem. Phys.*, 1974, **61**, 638.
30 D. Reinen and S. Krause, *Inorg. Chem.*, 1980, **20**, 2750.
31 M. A. Hitchman, *J. Chem. Soc. A*, 1970, 4.
32 F. S. Ham, *Phys. Rev. A*, 1965, **138**, 1727; 1968, **166**, 307.
33 C. E. Schäffer, *Pure Appl. Chem.*, 1970, **24**, 361 and refs. therein.
34 D. A. Cruse, J. E. Davies, M. Gerloch, J. H. Harding, D. J. Mackey and R. F. McMeecking, CAMMAG, A FORTRAN Computing Package, University Chemical Laboratory, Cambridge, 1979.
35 M. A. Hitchman, *Inorg. Chem.*, 1982, **21**, 821.
36 D. W. Smith, *Inorg. Chim. Acta*, 1977, **22**, 107.
37 R. G. McDonald and M. A. Hitchman, *Inorg. Chem.*, 1990, **29**, 3081 and refs. therein.

Received 9*th May* 1995; *Paper* 5/02929E